CHEMMEDCHEM

DOI: 10.1002/cmdc.200900468

Improved Model of Lanosterol 14α-Demethylase by Ligand-Supported Homology Modeling: Validation by Virtual Screening and Azole Optimization

Chunquan Sheng,[a] Wenya Wang,[a] Xiaoying Che,[a] Guoqiang Dong,[a] Shengzheng Wang,[a] Haitao Ji,[b] Zhenyuan Miao,[a] Jianzhong Yao,[a] and Wannian Zhang*[a]

Lanosterol 14α-demethylase (CYP51) is an important target for antifungal drugs. An improved three-dimensional model of CYP51 from *Candida albicans* (CACYP51) was constructed by ligand-supported homology modeling and molecular dynamics simulations. The accuracy of the constructed model was evaluated by its performance in a small-scale virtual screen. The results show that known CYP51 inhibitors were efficiently discriminated by the model, and it performed better than our previous CACYP51 model. The active site of CACYP51 was characterized by multiple copy simultaneous search (MCSS) calculations. On the basis of the MCSS results, a series of novel azoles were designed and synthesized, and they showed good in vitro antifungal activity with a broad spectrum. The MIC_{80} value of four of these compounds against *C. albicans* is 0.001 μg mL^{-1}, indicating that they are promising leads for the discovery of novel antifungal agents.

Introduction

Lanosterol 14α-demethylase ($P450_{14DM}$, CYP51) is a member of the cytochrome P450 superfamily, which catalyzes the oxidative removal of the 14α-methyl group (C32) of lanosterol to give $\Delta^{14,15}$-desaturated intermediates in ergosterol biosynthesis.[1] As an essential enzyme in the fungal life cycle, CYP51 has been a primary target for the azole class of antifungal agents. Eukaryotic CYP51 enzymes are membrane-associated proteins, and thus collecting crystal structure data remains a challenge. In the absence of structural information, homology modeling has proven to be an effective alternative for constructing reasonable three-dimensional (3D) protein models.

The incidence of systemic fungal infections has been increasing dramatically in recent years, and CYP51 represents an attractive target for antifungal therapy. In an attempt to design highly potent CYP51 inhibitors, we constructed a 3D model of CYP51 from *Candida albicans* (CACYP51) through homology modeling on the basis of the crystallographic coordinates of four prokaryotic P450 proteins (P450BM3, P450cam, P450terp, and P450eryF) and CYP51 from *Mycobacterium tuberculosis* (MTCYP51).[2,3] Detailed docking analysis led to a better understanding of the important interactions between CACYP51 and azole antifungal agents.[3,4] From the results of molecular modeling, successful structure-based optimization of azole antifungal agents has been reported by our research group.[4] Moreover, novel non-azole lead compounds were designed and synthesized by a structure-based de novo design approach.[5] However, the sequence identity between CACYP51 and the template protein is relatively low (29.5% for the whole protein and 30.5% for binding site residues). The efficiency of structure-based design of antifungal inhibitors is limited by the use of molecular models from traditional homology modeling methods. Therefore, building a more accurate model of CACYP51 is of great importance.

Evers, Gohlke, and Klebe developed a new approach toward homology modeling termed MOBILE,[6] which incorporates experimental information available from site-directed mutagenesis or structure–activity relationship (SAR) studies in the process of homology modeling and model refinement. Traditional homology methods only consider structural information available from template proteins, while the MOBILE approach uses the bound ligand molecules as spatial restraints and optimizes the initial homology models iteratively by incorporating the binding information of bioactive ligands. MOBILE has been successfully used to construct reasonable 3D models of several GPCR proteins,[7–9] and this method has been validated by structure-based ligand design and virtual screening. Moreover, several new methods for ligand-supported homology modeling have extended the methodology of the MOBILE approach.[10–11]

In the present study, we built an improved 3D model of CACYP51 by ligand-supported homology modeling and molecular dynamics (MD) simulation. The active site was characterized by multiple copy simultaneous search (MCSS)[12] calcula-

[a] *Dr. C. Sheng, Dr. W. Wang, Dr. X. Che, G. Dong, S. Wang, Dr. Z. Miao, Dr. J. Yao, Prof. W. Zhang*
School of Pharmacy, Military Key Laboratory of Medicinal Chemistry
Second Military Medical University
325 Guohe Road, Shanghai 200433 (People's Republic of China)
Fax: (+86) 21-81871243
E-mail: zhangwnk@hotmail.com

[b] *Dr. H. Ji*
Department of Chemistry
Department of Biochemistry, Molecular Biology, and Cell Biology
and Center for Drug Discovery and Chemical Biology
Northwestern University, Evanston, IL 60208-3113 (USA)

Supporting information for this article is available on the WWW under http://dx.doi.org/10.1002/cmdc.200900468.

tions. The reliability of the model was validated by a virtual screening test and structure-based optimization of azole antifungal agents. To the best of our knowledge, this is the first application of ligand-supported homology modeling to cytochrome P450 proteins.

Results and Discussion

Chemistry

The syntheses of compounds **8a–k** and **9a–c** are outlined in Schemes 1 and 2, respectively. The oxirane intermediate **4** was synthesized according to our reported procedure.[4] The *N*-methyl-substituted phenoxypropan-1-amine side chains **7a–k** were synthesized via two steps. Various substituted phenols were treated with excess 1,3-dibromopropane to give 1-(3-bromopropoxy)-substituted benzenes **6a–k**. These were subsequently reacted with methylamine in ethanol at room temperature to afford side chains **7a–k**. The target compounds **8a–k** were obtained in moderate to high yields by treating epoxide **4** with side chains **7a–k** in the presence of triethylamine and ethanol at 80 °C. Compounds **9a–c** were obtained by the reduction of the nitro groups of compounds **8j–k** in the presence of Raney nickel and hydrazine hydrate (Scheme 2). All the target compounds were obtained as racemates.

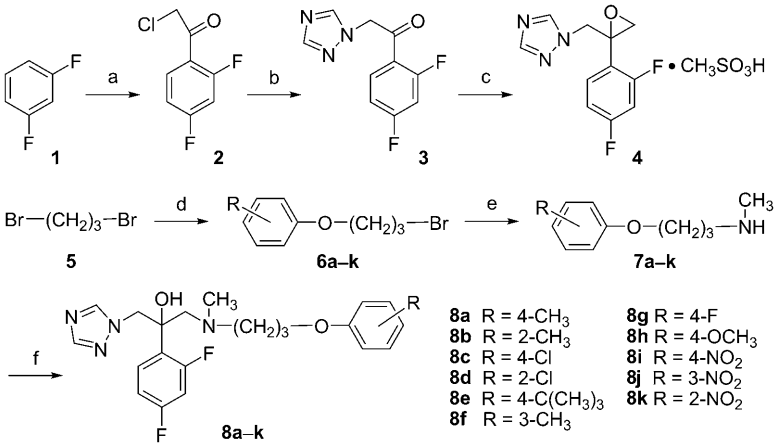

Scheme 1. Reagents and conditions: a) $ClCH_2COCl$, $AlCl_3$, CH_2Cl_2, 40 °C, 3 h, 50%; b) triazole, K_2CO_3, CH_2Cl_2, RT, 24 h, 70.0%; c) $(CH_3)_3SOI$, NaOH, toluene, 60 °C, 3 h, 62.3%; d) phenol, K_2CO_3, DMF, 70 °C, 2 h, 91.8–92.3%; e) methylamine alcohol solution, RT, 12 h, 97–98%; f) **4**, Et_3N, EtOH, reflux, 9 h, 44.4–58.5%.

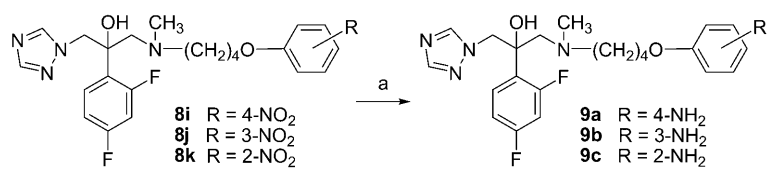

Scheme 2. Reagents and conditions: a) Raney Ni, NH_2NH_2, EtOH, RT, 5 h, 95.5–97.0%.

Generation of a ligand-supported homology model of CACYP51

For generation and validation of a ligand-supported homology model, details about the interaction between protein and ligand should be available.[6] In our previous studies, we generated a topographical interaction model[4] between azole inhibitors and CACYP51 (Figure 1) to guide the subsequent homology modeling process. The robustness of the interaction model has been validated by SAR studies[4,13] and site-directed mutagenesis.[14] In comparison with our previous homology modeling studies on CACYP51, a more accurate structure of MTCYP51 (PDB ID: 2VKU)[15] was used as the template. A set of 100 initial crude models of CACYP51 were generated by using the MODELLER module within the Insight II 2000 software package.[16] An azole inhibitor was then docked into each individual CACYP51 model by using the flexible docking method, Affinity.[17] The appropriate docking poses were determined by the interaction energies of Affinity and those calculated by the Cscore module of Sybyl 6.9.[18] To decrease search space, the active site was kept rigid during the docking study. On the basis of the ensemble CACYP51–azole complex, the best model was identified by the following selection criteria: 1) the model with the lowest interaction energy, 2) avoidance of any intramolecular clashes,[6] and 3) the generated binding mode of the azole compound with CACYP51 should agree with the derived ligand binding mode shown in Figure 1. After energy minimization, the resulting protein–ligand complex was further refined by MD simulation using the Charmm module[19] within the Insight II 2000 software package. The objective of the MD simulations was to relieve the structural strain stemming from the replacement of non-conserved residues in the homology modeling process and to obtain a reasonable conformation. From the deviation of the total energy and heavy atom RMSD during 1 ns MD simulations (see the Supporting Information), the total energy of the model decreased substantially in the first 100 ps of MD simulation and was stabilized after 300 ps equilibration.

Model validation through small-scale virtual screening

Structure-based virtual screening was performed with the refined CACYP51 model (Figure 2) to determine whether it could differentiate the known CACYP51 ligands from the "drug-like" decoy ligands. Following a well-accepted approach,[20] we constructed a test set containing 950 drug-like molecules extracted from the MDDR (MDL Drug Data Report) dataset and 32 known CACYP51 inhibitors with different scaffolds (the dataset is given in the Supporting Information). All the compounds in the test set were docked into the CACYP51 model with FlexX[21] and scored with four different scoring functions (D_Score,[22] ChemScore,[23] PMF,[24] and G_Score[25]) as implemented in the Cscore module of Sybyl 6.9. The en-

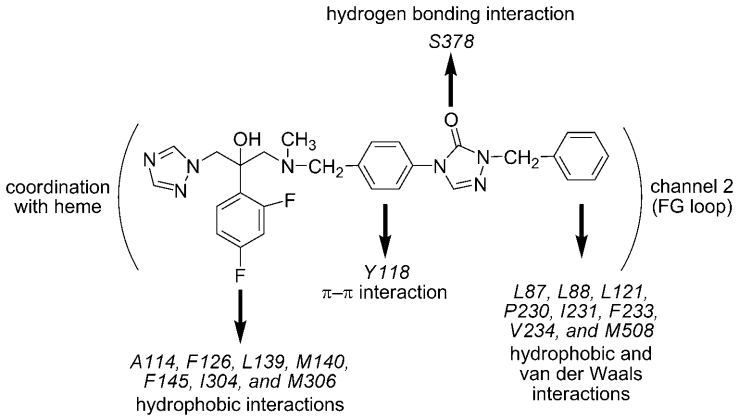

Figure 1. Schematic representation of the postulated interactions between CACYP51 and the azole compound (derived from ref. [4]); the arrows indicate proposed key interactions between receptor and ligand.

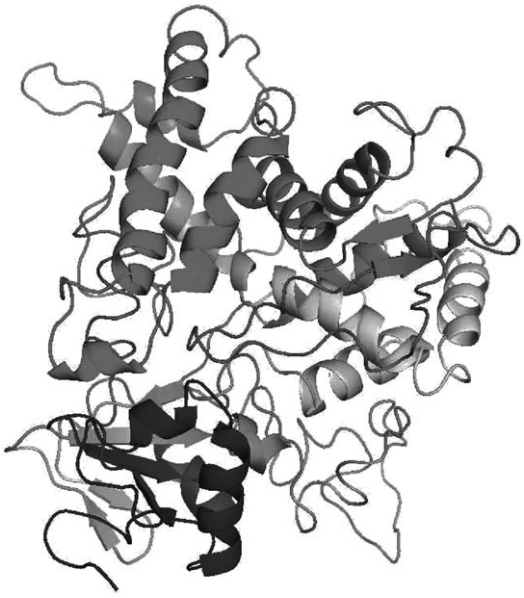

Figure 2. Ribbon representation of the refined homology model of CACYP51.

richment factor (EF) is plotted representing the fraction of the database that is screened versus the percentage of the active compounds found (Figure 3 A). The best result is obtained with PMF as the scoring function; analysis of the top 30 and 45% of the scored dataset results in 81 and 100% of the CYP51 inhibitors being identified. To compare the effectiveness of virtual screening between the present model and our previous 3D structure of CACYP51,[3] EF was also plotted with PMF as the scoring function (Figure 3 B). The structure constructed in this study performed better than the previous model, which suggests that ligand-supported homology modeling is more efficient when the sequence identity is relatively low between the template protein and the target protein. The above results also indicate that the present structure is suitable for virtual screening.

MCSS functional maps for the active site of CACYP51

To explore the key regions in the active site that are important for ligand binding, the MCSS program[12] was employed to calculate energetically favorable positions and orientations of given functional groups in the active site. The total numbers and ranges of energies of the minima found for the various molecular probes are summarized in Table 1. All of the energy minima of the ring functional groups (such as hydrophobic benzene and cyclohexane) were distributed over the S2 (above the heme ring), S3, and S4 (near the FG loop) subsites. Moreover, alkyl probes (such as propyl and *n*-butyl) revealed the same distribution profile. Polar groups (such as methanol, ethanol, and water) were mainly scattered over the S1 and S4 subsites (surrounding His 377 and Ser 378). The energy minima of the polar group can form hydrogen bonds His 310 (S1), Thr 311 (S1), and Ser 378 (S4), indicating that they are important hydrogen bonding (HB) sites. In combination with our previous modeling studies,[2–5] the active site of CACYP51 can be divided into four functional regions (Figure 4): 1) The S1 subsite represents the hydrophilic hydrogen bond binding site. His 310 and Thr 311 are two important HB sites in this area. 2) The S2 subsite is above the heme ring representing the core hydrophobic area. Hydrophobic scaffolds of the inhibitors (such as the sterol group of the substrate) or groups that coordinate with the heme (such as the triazole or imidazole group of the azole inhibitors) are favorable in this pocket. 3) The S3 subsite represents the narrow and hydrophobic cleft (facing the BC loop). The alkyl side chain (such as that of the substrate and chromene inhibitors) or substituted phenyl

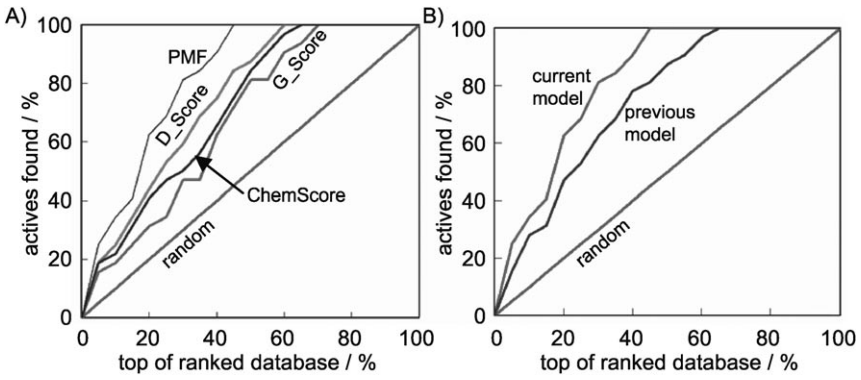

Figure 3. Enrichment of CYCYP51 obtained from: A) four different scoring functions and B) the new and previous homology models of CACYP51.

Table 1. Summary of results for the functional groups used in the MCSS calculations.

Functional Groups[a]	$\Delta H/2$ [kcal mol^{-1}]	Initial Number of Copies	Minima with $E_{interaction} < 0$	E Range [kcal mol^{-1}]	Minima with Interaction $< \Delta H/2$
BENZ	−3.80	1000	48	−2.72 ~ −22.51	43
CHEX	−3.97	1000	190	−0.01 ~ −9.09	73
PRPN	−2.69	1000	176	−0.28 ~ −8.00	171
ILER	−3.10	1000	343	−5.33 ~ −8.81	343
PHEN	−6.80	1000	235	−8.91 ~ −30.19	235
MEOH	−5.32	1000	162	−0.41 ~ −37.18	142
THRR	−6.26	1000	416	−5.37 ~ −26.13	89
WATR	−4.99	1000	195	−0.10 ~ −42.16	153

[a] MCSS functional groups: BENZ = benzene, CHEX = cyclohexane, PRPN = propane, ILER = butane, PHEN = phenol, MEOH = methanol, THRR = ethanol, WATR = water.

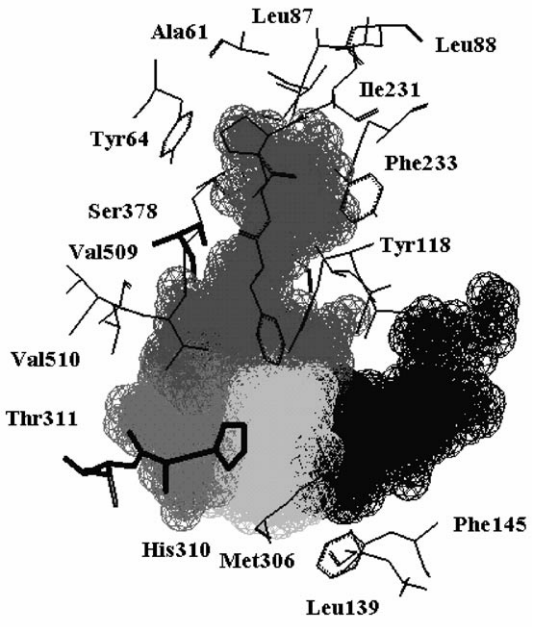

Figure 4. Surface rendering of the active site of CACYP51: the S1 site is at lower left; the S2 site is the region in the lower middle; the region at lower right is the S3 site; and at top is the S4 site.

groups (such as the difluorophenyl phenyl group of fluconazole) can form hydrophobic and van der Waals interactions with this region. 4) The S4 subsite represents a hydrophobic hydrogen bond binding site (facing the FG loop), which is important for the optimization of the C3 side chain of azole antifungal agents. A hydrophobic side chain is favorable in this region, and the addition of a group forming a HB interaction with Ser 378 can improve the affinity for CACYP51. In comparison with the MCSS calculation results of our previous model,[5] the four functional subsites are identical. The difference between them is the orientation of several residues in the active site (such as Tyr 118 and Ser 378), which resulted in the improved performance of the present model in virtual screening. The results from MCSS calculation can provide important information for the design of novel antifungal agents.

Structure-based azole optimization

To verify the reliability of the binding site characterization of CACYP51, a series of novel azoles were designed and synthesized on the basis of the four functional pockets in the active site. The triazole ring (located in the S2 subsite), difluorophenyl group (located in the S3 subsite), and C2 hydroxy group (located in the S1 subsite) are common scaffold components of triazole antifungal agents. *N*-Methyl-*N*-phenoxyalkylamines were designed as the side chains attached to C3. The steric and hydrophobic nature of this new type of side chain fits well with the S4 subsite. Moreover, the oxygen atom of the phenoxy group can function as a HB acceptor and form a HB interaction with Ser 378.

The in vitro antifungal activities of the synthesized compounds are listed in Table 2. The antifungal activity of each compound is expressed as the minimal inhibitory concentration (MIC) that effects 80% inhibition of the tested fungi, with fluconazole, itraconazole, and voriconazole used as reference drugs. In general, all the target compounds show excellent activity against most of the tested fungal pathogens except *A. fumigatus*. They show the greatest activity against *C. albicans* and *C. tropicalis*. Most of the compounds are more potent than fluconazole, itraconazole, and voriconazole, with MIC_{80} values in the range of 0.016–0.001 μg mL^{-1}. On the *C. neoformans* strain, the inhibitory activities of the target compounds are similar or superior to that of fluconazole. In particular, the inhibitory activity of compound **8c** ($MIC_{80} = 0.004$ μg mL^{-1}) is fourfold higher than that of voriconazole. Fluconazole is not effective against *A. fumigatus*, whereas some of our compounds show moderate activity. For example, the MIC_{80} value of compound **8i** against *A. fumigatus* is 16 μg mL^{-1}; however, it is less active than itraconazole and voriconazole. For the dermatophytes (i.e., *T. rubrum* and *M. gypseum*), most of the compounds show moderate to good inhibitory activity. They reveal higher inhibitory activity against *M. gypseum* than against *T. rubrum*. Several compounds (such as compounds **8a** and **8b**) are more active than the reference antifungal drugs. Among the synthesized triazoles, compounds **8a**, **8c**, **8f**, and **8i** exhibit strong in vitro antifungal activity with a broad antifungal spectrum, and are worthy of further evaluation.

To clarify the binding mode and SAR of the synthesized azoles, compound **8i** was docked into the active site of CACYP51. The result revealed that compound **8i** binds CACYP51 with an extended conformation (Figure 5). The C2 hydroxy group, triazole ring, and difluorophenyl group are located in the S1, S2, and S3 subsites, respectively. They form similar interactions with CACYP51 as observed in the docking model of fluconazole.[4] The substituted alkoxybenzene side chain is oriented into the S4 pocket. The *N*-methyl group of

Table 2. In vitro antifungal activities of the triazole compounds.[a]

Compd	MIC_{80} [$\mu g\,mL^{-1}$]					
	C. alb.	*C. tro.*	*C. neo.*	*T. rub.*	*M. gyp.*	*A. fum.*
8a	0.001	0.004	0.0625	0.0625	0.25	64
8b	0.004	0.16	0.0625	0.25	0.625	>64
8c	0.001	1	0.004	0.25	0.0625	64
8d	0.004	0.016	0.0625	0.25	0.0625	>64
8e	0.016	0.0625	0.0625	1	0.25	64
8f	0.001	0.004	0.25	0.25	0.0625	>64
8g	0.004	0.016	0.25	1	0.25	>64
8h	0.016	0.016	0.0625	1	0.0625	64
8i	0.001	1	0.25	0.25	0.0625	16
8j	0.004	0.0625	0.25	1	0.25	>64
8k	0.004	0.016	0.25	4	0.0625	>64
9a	0.016	0.0625	1	4	1	>64
9b	0.0625	16	1	4	0.25	>64
9c	0.0625	0.0625	1	1	0.25	>64
FLZ	0.5	0.25	1	4	0.0625	>64
ITZ	0.0625	0.016	0.125	0.125	0.0625	2
VOR	0.016	0.016	0.016	0.0625	0.0625	0.25

[a] Abbreviations: *C. alb.* = *Candida albicans*, *C. tro.* = *Candida tropicalis*, *C. neo.* = *Cryptococcus neoformans*, *T. rub.* = *Trichophyton rubrum*, *M. gyp.* = *Microsporum gypseum*, *A. fum.* = *Aspergillus fumigatus*; FLZ = fluconazole, ITZ = itraconazole, VOR = voriconazole.

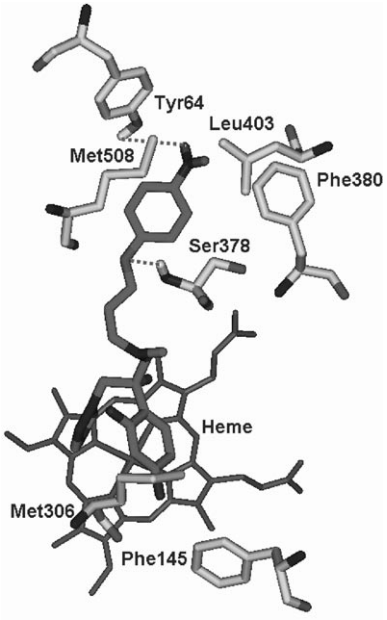

Figure 5. The docking conformation of compound **8i** in the active site of CACYP51: Important residues that interact with **8i** are indicated, and hydrogen bonds are represented by dashed lines. The image was generated with the Insight II 2000 software package.

the side chain forms hydrophobic and van der Waals interactions with Phe228. The propyl group forms hydrophobic and van der Waals interactions with Leu376, Ile379, Leu461, and Val519. The oxygen atom is hydrogen bonded with Ser378. The terminal phenyl group is located in a hydrophobic pocket lined by Tyr64, Phe380, Leu403, and Met508. Small hydrophobic substituents on the phenyl group can improve the affinity of the compounds for CACYP51. For example, compounds **8a**, **8c**, and **8f** showed excellent antifungal activity. The nitro group of compound **8i** forms hydrogen bonds with the hydroxy group of Tyr64. The hydrogen bonds would be broken if the 4-nitro group of compound **8i** were moved to positions 3 or 2 (compounds **8j** and **8k**, respectively), or reduced to an amino group (compound **9a**), which resulted in a 4–16-fold decrease in antifungal activity.

Conclusions

In summary, ligand-supported homology modeling is a useful method to build accurate 3D structures of proteins when the sequence identity between the template structure and the target protein is low. An improved model of CACYP51 was built by ligand-supported homology modeling. The current model has several advantages over the previous homology model of CACYP51.[2,3] First, the ligand information was taken into account in the construction of the molecular model, and MD simulations were used in model refinement; this ensures a reasonable 3D structure with low energy. Second, the CACYP51 model performs well in the virtual screening test, which is beneficial for finding lead structures. Lastly, the active site of CACYP51 model was characterized by MCSS calculations. The results reveal its efficiency in structure-based optimization of novel azole antifungal agents. The new azoles designed show excellent activity with a broad antifungal spectrum. In particular, the MIC_{80} values of the most active compounds **8a**, **8c**, **8d**, and **8i** against *C. albicans* reach 0.001 $\mu g\,mL^{-1}$. These compounds are more potent than fluconazole, itraconazole, and voriconazole, and are promising leads for the development of novel antifungal agents. Based on the above results, it is anticipated that the improved homology model of CACYP51 could be used as a suitable template for the structure-based design of novel inhibitors.

Experimental Section

Chemistry

General methods: NMR spectra were recorded on a Bruker 500 spectrometer with $(CH_3)_4Si$ as internal standard and $CDCl_3$ as solvent. Chemical shift (δ) values and coupling constants (J) are given in ppm and Hz, respectively. ESI mass spectra were performed on an API-3000 LC–MS instrument. High-resolution mass spectrometry data were collected on a Kratos Concept mass spectrometer. Elemental analyses were performed with a MOD-1106 instrument and are consistent with theoretical values within $\pm 0.4\%$. TLC analysis was carried out on silica gel plates GF_{254} (Qindao Haiyang Chemical, China). Column chromatography was performed with silica gel

60 G (Qindao Haiyang Chemical, China). Commercial solvents were used without pretreatment.

1-(3-Propanoxy)-4-methylbenzene (6a): A solution of *p*-cresol (10.81 g, 0.10 mol) in DMF (50 mL) was added dropwise to a stirred suspension of 1,3-dibromopropane (40.38 g, 0.20 mol) and K_2CO_3 (20.73 g, 0.15 mol) in DMF (100 mL) at room temperature. The reaction mixture was then stirred at room temperature for 2 h, and heated at 70 °C for 2 h. The mixture was filtered, and the resulting solution was diluted with EtOAc (200 mL) and washed with H_2O (3×100 mL). The organic layer was separated, dried with anhydrous Na_2SO_4, and concentrated under reduced pressure. The residue was purified by column chromatography (hexane) to give **6a** as a colorless oil (21.04 g, 92.3%). ^{1}H NMR (500 MHz, $CDCl_3$): δ = 6.80–7.09 (m, 4H), 4.07 (t, J = 5.8 Hz, 2H), 3.60 (t, J = 6.5 Hz, 2H), 2.30–2.34 (m, 2H), 2.28 ppm (s, 3H); MS (ESI) *m/z*: 229 [*M*+1]. The syntheses of the subsequent compounds **6b**–**k** were carried out similarly to that of compound **6a**.

***N*-Methyl-3-(*p*-tolyloxy)propan-1-amine (7a):** A solution of compound **6a** (3.42 g, 0.015 mol) in EtOH (20 mL) was added dropwise to a solution of methylamine alcohol (40 mL). The mixture was stirred at room temperature for 12 h, at which time the reaction was nearly complete. The solvent was evaporated under reduced pressure to give **7a** as a white solid (2.60 g, 97%). The product was used in the next step without further purification. ^{1}H NMR (500 MHz, $CDCl_3$): δ = 6.77–7.09 (m, 4H), 3.97 (t, J = 6.2 Hz, 2H), 2.94 (t, J = 7.3 Hz, 2H), 2.53 (s, 3H), 2.27 (s, 3H), 1.93–1.95 ppm (m, 2H); MS (ESI) *m/z*: 180 [*M*+1]. The syntheses of the subsequent compounds **7b**–**k** were carried out similarly to that of compound **7a**.

2-(2,4-Difluorophenyl)-3-{methyl-[3-(*p*-tolyloxy)propyl]amino}-1-(1*H*-1,2,4-triazol-1-yl)propan-2-ol (8a): A solution of epoxide **4** (1.67 g, 0.005 mol), **7a** (1.08 g, 0.006 mol), Et_3N (3 mL), and EtOH (30 mL) was heated at reflux for 9 h. The solvent was evaporated under reduced pressure. The residue was purified by silica gel column chromatography (CH_2Cl_2/MeOH 100:2, *v/v*) to give **8a** as a pale-yellow oil (1.20 g, 57.7%). R_f = 0.27 (CH_2Cl_2/MeOH 50:1); ^{1}H NMR (500 MHz, $CDCl_3$): δ = 8.10 (s, 1H), 7.76 (s, 1H), 6.74–7.52 (m, 7H), 5.30 (br, 1H), 4.52 (d, J = 14.3 Hz, 1H), 4.47 (d, J = 14.2 Hz, 1H), 3.85 (t, J = 6.0 Hz, 2H), 3.05 (d, J = 13.4 Hz, 1H), 2.76 (d, J = 13.3 Hz, 1H), 2.51 (br, 2H), 2.29 (s, 3H), 2.08 (s, 3H), 1.74–1.76 ppm (m, 2H); ^{13}C NMR (500 MHz, $CDCl_3$): δ = 162.56, 158.84, 156.47, 150.81, 144.57, 129.87, 129.48, 126.17, 114.20, 111.31, 104.02, 72.14, 65.29, 62.33, 56.27, 55.73, 43.55, 26.96, 20.32 ppm; HRMS-FAB *m/z* [*M*+H]$^+$: calcd for $C_{22}H_{26}F_2N_4O_2$: 417.2024, found: 417.12020; Anal. calcd for $C_{22}H_{26}F_2N_4O_2$: C 63.45, H 6.29, N 13.45, found: C 63.26, H 6.31, N 13.49. The syntheses of the subsequent compounds **8b**–**k** were carried out similarly to that of compound **8a**.

3-{[3-(4-Aminophenoxy)propyl](methyl)amino}-2-(2,4-difluorophenyl)-1-(1*H*-1,2,4-triazol-1-yl)propan-2-ol (9a): Raney Ni (cat.) was added to a solution of **8j** (0.89 g, 2 mmol) in EtOH (25 mL) in the presence of N_2H_4 (5 mL). The mixture was stirred at room temperature for 5 h. The solid was separated, and the filtrate was evaporated under reduced pressure. The residue was purified by column chromatography (CH_2Cl_2/MeOH 100:2, *v/v*) to give **9a** as a yellow oil (0.79 g, 95.5%). R_f = 0.08 (CH_2Cl_2/MeOH 50:1); ^{1}H NMR (500 MHz, $CDCl_3$): δ = 8.10 (s, 1H), 7.76 (s, 1H), 6.63–7.52 (m, 7H), 5.30 (br, 1H), 4.50 (d, J = 14.2 Hz, 2H), 3.81 (t, J = 6.0 Hz, 2H), 3.06 (d, J = 13.3 Hz, 1H), 2.79 (d, J = 13.6 Hz, 1H), 2.54 (br, 2H), 2.10 (s, 3H), 1.73–1.76 ppm (m, 2H); HRMS-FAB *m/z* [*M*+H]$^+$: calcd for $C_{21}H_{25}F_2N_5O_2$: 418.1976, found: 418.1980; Anal. calcd for $C_{21}H_{25}F_2N_5O_2$: C 60.42, H 6.04, N 16.78, found: C 60.54, H 6.05, N 16.72. The syntheses of the subsequent compounds **9b** and **9c** were carried out similarly to that of compound **9a**.

2-(2,4-Difluorophenyl)-3-{methyl-[3-(*o*-tolyloxy)propyl]amino}-1-(1*H*-1,2,4-triazol-1-yl)propan-2-ol (8b): Pale-yellow oil. R_f = 0.30 (CH_2Cl_2/MeOH 50:1); ^{1}H NMR (500 MHz, $CDCl_3$): δ = 8.08 (s, 1H), 7.77 (s, 1H), 6.75–7.51 (m, 7H), 5.30 (br, 1H), 4.49 (d, J = 14.2 Hz, 2H), 3.87 (t, J = 6.0 Hz, 2H), 3.05 (d, J = 13.6 Hz, 1H), 2.76 (d, J = 13.6 Hz, 1H), 2.55 (t, J = 6.8 Hz, 2H), 2.16 (s, 3H), 2.09 (s, 3H), 1.77–1.80 ppm (m, 2H); HRMS-FAB *m/z* [*M*+H]$^+$: calcd for $C_{22}H_{26}F_2N_4O_2$: 417.2024, found: 417.12018; Anal. calcd for $C_{22}H_{26}F_2N_4O_2$: C 63.45, H 6.29, N 13.45, found: C, 63.70; H, 6.31; N, 13.40.

1-{[3-(4-Chlorophenoxy)propyl](methyl)amino}-2-(2,4-difluorophenyl)-1-(1*H*-1,2,4-triazol-1-yl)propan-2-ol (8c): Pale-yellow oil. R_f = 0.11 (CH_2Cl_2/MeOH 50:1); ^{1}H NMR (500 MHz, $CDCl_3$): δ = 8.13 (s, 1H), 7.79 (s, 1H), 6.76–7.52 (m, 7H), 5.31 (br, 1H), 4.50 (d, J = 14.2 Hz, 2H), 3.83 (t, J = 5.8 Hz, 2H), 3.05 (d, J = 13.4 Hz, 1H), 2.74 (d, J = 13.6 Hz, 1H), 2.49 (br, 2H), 2.06 (s, 3H), 1.75 ppm (br, 2H); HRMS-FAB *m/z* [*M*+H]$^+$: calcd for $C_{21}H_{23}ClF_2N_4O_2$: 437.1478, found: 437.1470; Anal. calcd for $C_{21}H_{23}ClF_2N_4O_2$: C 57.73, H 5.31, N 12.82, found: C 57.84, H 5.29, N 12.84.

1-{[3-(2-Chlorophenoxy)propyl](methyl)amino}-2-(2,4-difluorophenyl)-1-(1*H*-1,2,4-triazol-1-yl)propan-2-ol (8d): Pale-yellow oil. R_f = 0.16 (CH_2Cl_2/MeOH 50:1); ^{1}H NMR (500 MHz, $CDCl_3$): δ = 8.08 (s, 1H), 7.76 (s, 1H), 6.75–7.36 (m, 7H), 4.50 (d, J = 14.2 Hz, 2H), 3.93 (t, J = 5.8 Hz, 2H), 3.05 (d, J = 13.6 Hz, 1H), 2.78 (d, J = 13.6 Hz, 1H), 2.57–2.60 (m, 2H), 2.10 (s, 3H), 1.80–1.83 ppm (m, 2H); HRMS-FAB *m/z* [*M*+H]$^+$: calcd for $C_{21}H_{23}ClF_2N_4O_2$: 437.1478, found: 437.1470; Anal. calcd for $C_{21}H_{23}ClF_2N_4O_2$: C 57.73, H 5.31, N 12.82, found: C 57.55, H 5.30, N 12.86.

1-{[3-(4-*tert*-Butylphenoxy)propyl](methyl)amino}-2-(2,4-difluorophenyl)-1-(1*H*-1,2,4-triazol-1-yl)propan-2-ol (8e): Pale-yellow oil. R_f = 0.16 (CH_2Cl_2/MeOH 50:1); ^{1}H NMR (500 MHz, $CDCl_3$): δ = 8.11 (s, 1H), 7.76 (s, 1H), 6.76–7.53 (m, 7H), 4.50 (d, J = 14.2 Hz, 2H), 3.95 (t, J = 5.8 Hz, 2H), 3.06 (d, J = 13.4 Hz, 1H), 2.80 (d, J = 13.6 Hz, 1H), 2.60 (br, 2H), 2.09 (s, 3H), 1.58 (br, 2H), 1.30 ppm (s, 9H); HRMS-FAB *m/z* [*M*+H]$^+$: calcd for $C_{25}H_{32}F_2N_4O_2$: 459.2493, found: 459.2489; Anal. calcd for $C_{25}H_{32}F_2N_4O_2$: C 65.48, H 7.03, N, 12.22, found: C 65.68, H 7.02, N 12.20.

2-(2,4-Difluorophenyl)-3-{methyl-[3-(*m*-tolyloxy)propyl]amino}-1-(1*H*-1,2,4-triazol-1-yl)propan-2-ol (8f): Pale-yellow oil. R_f = 0.17 (CH_2Cl_2/MeOH 50:1); ^{1}H NMR (500 MHz, $CDCl_3$): δ = 8.16 (s, 1H), 7.77 (s, 1H), 6.66–7.57 (m, 7H), 5.30 (br, 1H), 4.53 (d, J = 14.2 Hz, 2H), 3.85 (br, 2H), 3.07 (d, J = 13.6 Hz, 1H), 2.76 (d, J = 13.6 Hz, 1H), 2.51 (br, 2H), 2.08 (s, 3H), 2.05 (s, 3H), 1.75 ppm (br, 2H); HRMS-FAB *m/z* [*M*+H]$^+$: calcd for $C_{22}H_{26}F_2N_4O_2$: 417.2024, found: 417.12028; Anal. calcd for $C_{22}H_{26}F_2N_4O_2$: C 63.45, H 6.29, N 13.45, found: C 63.25, H 6.28, N 13.50.

2-(2,4-Difluorophenyl)-3-{[3-(4-fluorophenoxy)propyl](methyl)amino}-1-(1*H*-1,2,4-triazol-1-yl)propan-2-ol (8g): Pale-yellow oil. R_f = 0.14 (CH_2Cl_2/MeOH 50:1); ^{1}H NMR (500 MHz, $CDCl_3$): δ = 8.13 (s, 1H), 7.78 (s, 1H), 6.76–7.54 (m, 7H), 4.49 (d, J = 14.2 Hz, 2H), 3.85 (t, J = 5.9 Hz, 2H), 3.07 (d, J = 13.6 Hz, 1H), 2.76 (d, J = 13.6 Hz, 1H), 2.52 (br, 2H), 2.08 (s, 3H), 1.76 ppm (br, 2H); HRMS-FAB *m/z* [*M*+H]$^+$: calcd for $C_{21}H_{23}F_3N_4O_2$: 421.1773, found: 421.1762; Anal. calcd for $C_{21}H_{23}F_3N_4O_2$: C 59.99, H 5.51, N 13.33, found: C 59.87, H 5.53, N 13.36.

2-(2,4-Difluorophenyl)-3-{[3-(4-methoxyphenoxy)propyl](methyl)amino}-1-(1*H*-1,2,4-triazol-1-yl)propan-2-ol (8h): Pale-yellow oil. R_f = 0.22 (CH_2Cl_2/MeOH 50:1); ^{1}H NMR (500 MHz, $CDCl_3$): δ = 8.12 (s, 1H), 7.77 (s, 1H), 6.77–7.52 (m, 7H), 5.30 (br, 1H, OH),

4.50 (d, J=14.2 Hz, 2H), 3.85 (t, J=6.0 Hz, 2H), 3.77 (s, 3H), 3.05 (d, J=13.2 Hz, 1H), 2.75 (d, J=13.3 Hz, 1H), 2.51 (br, 2H), 2.08 (s, 3H), 1.75 ppm (br, 2H); ^{13}C NMR (500 MHz, $CDCl_3$): δ=162.58, 158.88, 157.27, 150.96, 144.65, 129.48, 129.31, 126.30, 125.65, 115.64, 111.41, 104.14, 72.09, 65.68, 62.19, 56.25, 55.70, 43.62, 26.91 ppm; HRMS-FAB m/z $[M+H]^+$: calcd for $C_{22}H_{26}F_2N_4O_3$: 433.1973, found: 433.1979; Anal. calcd for $C_{22}H_{26}F_2N_4O_3$: C 61.10, H 6.06, N 12.96, found: C 60.92, H 6.08, N 12.93.

2-(2,4-Difluorophenyl)-3-{methyl-[3-(4-nitrophenoxy)propyl]amino}-1-(1*H*-1,2,4-triazol-1-yl)propan-2-ol (8i): Pale-yellow oil. R_f= 0.11 (CH_2Cl_2/MeOH 50:1); ^{1}H NMR (500 MHz, $CDCl_3$): δ=8.13 (s, 1H), 7.80 (s, 1H), 6.77–7.56 (m, 7H), 5.25 (br, 1H), 4.50 (d, J= 14.2 Hz, 2H), 3.94 (t, J=5.9 Hz, 2H), 3.07 (d, J=13.5 Hz, 1H), 2.76 (d, J=13.7 Hz, 1H), 2.50 (t, J=6.6 Hz, 2H), 2.09 (s, 3H), 1.78–1.81 ppm (m, 2H); ^{13}C NMR (500 MHz, $CDCl_3$): 163.63, 162.68, 158.84, 150.97, 144.67, 141.49, 129.41, 126.23, 125.85, 114.28, 111.44, 104.20, 72.06, 66.28, 62.00, 56.13, 55.50, 43.66, 26.72 ppm; HRMS-FAB m/z $[M+H]^+$: calcd for $C_{21}H_{23}F_2N_5O_4$: 448.1718, found: 448.1709; Anal. calcd for $C_{21}H_{23}F_2N_5O_4$: C 56.37, H 5.18, N 15.65, found: C 56.48, H 5.19, N 15.60.

2-(2,4-Difluorophenyl)-3-{methyl-[3-(3-nitrophenoxy)propyl]amino}-1-(1*H*-1,2,4-triazol-1-yl)propan-2-ol (8j): Pale-yellow oil. R_f= 0.19 (CH_2Cl_2/MeOH 50:1); ^{1}H NMR (500 MHz, $CDCl_3$): δ=8.12 (s, 1H), 7.79 (s, 1H), 6.81–7.82 (m, 7H), 5.29 (br, 1H), 4.51 (d, J= 14.2 Hz, 2H), 3.93 (t, J=6.0 Hz, 2H), 3.09 (d, J=13.5 Hz, 1H), 2.77 (d, J=13.6 Hz, 1H), 2.52 (t, J=6.6 Hz, 2H), 2.11 (s, 3H), 1.79–1.82 ppm (m, 2H); ^{13}C NMR (500 MHz, $CDCl_3$): 162.45, 159.09, 158.90, 150.80, 148.99, 144.54, 129.82, 129.35, 126.12, 121.33, 115.61, 111.28, 108.50, 104.02, 72.07, 66.05, 62.06, 56.08, 55.44, 43.55, 26.63 ppm; HRMS-FAB m/z $[M+H]^+$: calcd for $C_{21}H_{23}F_2N_5O_4$: 448.1718, found: 448.1706; Anal. calcd for $C_{21}H_{23}F_2N_5O_4$: C 56.37, H 5.18, N 15.65, found: C 56.26, H 5.19, N 15.68.

2-(2,4-Difluorophenyl)-3-{methyl-[3-(2-nitrophenoxy)propyl]amino}-1-(1*H*-1,2,4-triazol-1-yl)propan-2-ol (8k): Pale-yellow oil. R_f= 0.28 (CH_2Cl_2/MeOH 50:1); ^{1}H NMR (500 MHz, $CDCl_3$): δ=8.09 (s, 1H), 7.76 (s, 1H), 6.76–7.85 (m, 7H), 5.30 (br, 1H), 4.50 (d, J= 14.2 Hz, 2H), 4.01 (br, 2H), 3.04 (d, J=13.2 Hz, 1H), 2.73 (d, J= 13.2 Hz, 1H), 2.52 (br, 2H), 2.10 (s, 3H), 1.78 ppm (br, 2H); HRMS-FAB m/z $[M+H]^+$: calcd for $C_{21}H_{23}F_2N_5O_4$: 448.1718, found: 448.1713; Anal. calcd for $C_{21}H_{23}F_2N_5O_4$: C 56.37, H 5.18; N 15.65, found: C 56.20, H 5.17, N 15.70.

1-{[3-(3-Aminophenoxy)propyl](methyl)amino}-2-(2,4-difluorophenyl)-1-(1*H*-1,2,4-triazol-1-yl)propan-2-ol (9b): Pale-yellow oil. R_f=0.11 (CH_2Cl_2/MeOH 50:1); ^{1}H NMR (500 MHz, $CDCl_3$): δ=8.10 (s, 1H), 7.77 (s, 1H), 6.17–7.26 (m, 7H), 5.30 (br, 1H), 4.50 (d, J= 14.2 Hz, 2H), 3.84 (t, J=5.9 Hz, 2H), 3.05 (d, J=13.2 Hz, 1H), 2.78 (d, J=13.2 Hz, 1H), 2.52 (br, 2H), 2.101 (s, 3H), 1.75 ppm (br, 2H); HRMS-FAB m/z $[M+H]^+$: calcd for $C_{21}H_{25}F_2N_5O_2$: 418.1976, found: 418.1967; Anal. calcd for $C_{21}H_{25}F_2N_5O_2$: C 60.42, H 6.04, N 16.78, found: C 60.24, H 6.06, N 16.75.

1-{[3-(2-Aminophenoxy)propyl](methyl)amino}-2-(2,4-difluorophenyl)-1-(1*H*-1,2,4-triazol-1-yl)propan-2-ol (9c): Pale-yellow oil. R_f=0.08 (CH_2Cl_2/MeOH 50:1); ^{1}H NMR (500 MHz, $CDCl_3$): δ=8.10 (s, 1H), 7.77 (s, 1H), 6.70–7.54 (m, 7H), 5.30 (br, 1H), 4.50 (d, J= 14.2 Hz, 2H), 3.91 (t, J=6.0 Hz, 2H), 3.07 (d, J=13.0 Hz, 1H), 2.80 (d, J=13.0 Hz, 1H), 2.55 (br, 2H), 2.11 (s, 3H), 1.81 ppm (br, 2H); HRMS-FAB m/z $[M+H]^+$: calcd for $C_{21}H_{25}F_2N_5O_2$: 418.1976, found: 418.1972; Anal. calcd for $C_{21}H_{25}F_2N_5O_2$: C 60.42, H 6.04, N 16.78, found: C 60.60, H 6.05, N 16.71.

***In vitro* antifungal activity assays**

In vitro antifungal activities are expressed as MIC_{80} values, and were measured by the serial dilution method in 96-well microtiter plates. Test fungal strains were either clinical isolates, or were obtained from the American Type Culture Collection (ATCC). MIC_{80} determinations were performed according to the National Committee for Clinical Laboratory Standards (NCCLS) recommendations, with RPMI 1640 (Sigma) buffered with 0.165 M MOPS (Sigma) as the test medium. The MIC_{80} value is defined as the lowest concentration of test compound that results in a culture with turbidity $\leq$80% inhibition relative to the growth of the control. Test compounds were dissolved in DMSO serially diluted in growth medium. The yeast strains were incubated at 35 °C, and the dermatophytes at 28 °C. Growth MIC_{80} was determined at 24 h for *Candida* spp., at 72 h for *Cryptococcus neoformans*, and at 7 days for filamentous fungi.

Acknowledgements

This work was supported by the National Natural Science Foundation of China (Grant No. 30930107), the Shanghai Rising-Star Program (Grant No. 09A1407000), the National Major Special Project for the Creation of New Drugs (Grant No. 2009ZX09301-011), and the Shanghai Leading Academic Discipline Project (Project No. B906).

Keywords: active sites · antifungal agents · azoles · cytochromes · homology modeling

[1] Y. Aoyama, Y. Yoshida, R. Sato, *J. Biol. Chem.* **1984**, *259*, 1661–1666.
[2] H. Ji, W. Zhang, Y. Zhou, M. Zhang, J. Zhu, Y. Song, J. Lu, *J. Med. Chem.* **2000**, *43*, 2493–2505.
[3] C. Sheng, W. Zhang, M. Zhang, Y. Song, H. Ji, J. Zhu, J. Yao, J. Yu, S. Yang, Y. Zhou, J. Lu, *J. Biomol. Struct. Dyn.* **2004**, *22*, 91–99.
[4] C. Sheng, W. Zhang, H. Ji, M. Zhang, Y. Song, H. Xu, J. Zhu, Z. Miao, Q. Jiang, J. Yao, Y. Zhou, J. Lu, *J. Med. Chem.* **2006**, *49*, 2512–2525.
[5] H. Ji, W. Zhang, M. Zhang, M. Kudo, Y. Aoyama, Y. Yoshida, C. Sheng, Y. Song, S. Yang, Y. Zhou, J. Lu, J. Zhu, *J. Med. Chem.* **2003**, *46*, 474–485.
[6] A. Evers, H. Gohlke, G. Klebe, *J. Mol. Biol.* **2003**, *334*, 327–345.
[7] A. Evers, T. Klabunde, *J. Med. Chem.* **2005**, *48*, 1088–1097.
[8] A. Evers, G. Klebe, *Angew. Chem.* **2003**, *115*, 250–253; *Angew. Chem. Int. Ed.* **2004**, *43*, 248–251.
[9] A. Evers, G. Klebe, *J. Med. Chem.* **2004**, *47*, 5381–5392.
[10] C. N. Cavasotto, A. J. Orry, N. J. Murgolo, M. F. Czarniecki, S. A. Kocsi, B. E. Hawes, K. A. O'Neill, H. Hine, M. S. Burton, J. H. Voigt, R. A. Abagyan, M. L. Bayne, F. J. Monsma, Jr., *J. Med. Chem.* **2008**, *51*, 581–588.
[11] A. Patny, P. V. Desai, M. A. Avery, *Proteins* **2006**, *65*, 824–842.
[12] A. Miranker, M. Karplus, *Proteins* **1991**, *11*, 29–34.
[13] F. Giraud, C. Loge, F. Pagniez, D. Crepin, P. Le Pape, M. Le Borgne, *Bioorg. Med. Chem. Lett.* **2008**, *18*, 1820–1824.
[14] S. H. Chen, C. Q. Sheng, X. H. Xu, Y. Y. Jiang, W. N. Zhang, C. He, *Biol. Pharm. Bull.* **2007**, *30*, 1246–1253.
[15] A. N. Eddine, J. P. von Kries, M. V. Podust, T. Warrier, S. H. Kaufmann, L. M. Podust, *J. Biol. Chem.* **2008**, *283*, 15152–15159.
[16] Insight II: Accelrys Inc., 2000: 10188 Telesis Court, Suite 100, San Diego, CA 92121 (USA); http://www.accelrys.com/ (accessed December 22, 2009).
[17] B. A. Luty, Z. R. Wasserman, P. F. W. Stouten, C. N. Hodge, M. Zacharias, J. A. McCammon, *J. Comput. Chem.* **1995**, *16*, 454–464.
[18] Tripos Associates Inc., 2001: St. Louis, MO (USA); http://www.tripos.com (accessed December 22, 2009).
[19] B. R. Brooks, R. E. Bruccoleri, B. D. Olafson, D. J. States, S. Swaminathan, M. Karplus, *J. Comput. Chem.* **1983**, *4*, 187–217.
[20] C. Bissantz, P. Bernard, M. Hibert, D. Rognan, *Proteins* **2003**, *50*, 5–25.

[21] M. Rarey, B. Kramer, T. Lengauer, G. Klebe, *J. Mol. Biol.* **1996**, *261*, 470 – 489.
[22] H. Gohlke, M. Hendlich, G. Klebe, *J. Mol. Biol.* **2000**, *295*, 337 – 356.
[23] M. D. Eldridge, C. W. Murray, T. R. Auton, G. V. Paolini, R. P. Mee, *J. Comput. Aided Mol. Des.* **1997**, *11*, 425 – 445.
[24] I. Muegge, Y. C. Martin, *J. Med. Chem.* **1999**, *42*, 791 – 804.
[25] G. Jones, P. Willett, R. C. Glen, A. R. Leach, R. Taylor, *J. Mol. Biol.* **1997**, *267*, 727 – 748.

Received: November 14, 2009
Revised: December 15, 2009
Published online on February 15, 2010

